SCIENTIFIC REPORTS

OPEN

SUBJECT AREAS:
OPTICS AND PHOTONICS
SLOW LIGHT
INTEGRATED OPTICS
PHOTONIC CRYSTALS

Received
5 August 2013

Accepted
3 December 2013

Published
18 December 2013

Correspondence and requests for materials should be addressed to A.O. (opheij@amolf.nl)

Ultracompact (3 μm) silicon slow-light optical modulator

Aron Opheij[1], Nir Rotenberg[1], Daryl M. Beggs[1,4], Isabella H. Rey[2], Thomas F. Krauss[2,3] & L. Kuipers[1]

[1]Center for Nanophotonics, FOM Institute AMOLF, Science Park 104, 1098 XG, Amsterdam, The Netherlands, [2]School of Physics and Astronomy, University of St Andrews, St Andrews, Fife, KY16 9SS, UK, [3]Department of Physics, University of York, York, YO10 5DD, UK, [4]Centre for Quantum Photonics, University of Bristol, HH Wills Physics Laboratory, Tyndall Avenue, Bristol BS8 1TL.

Wavelength-scale optical modulators are essential building blocks for future on-chip optical interconnects. Any modulator design is a trade-off between bandwidth, size and fabrication complexity, size being particularly important as it determines capacitance and actuation energy. Here, we demonstrate an interesting alternative that is only 3 μm long, only uses silicon on insulator (SOI) material and accommodates several nanometres of optical bandwidth at 1550 nm. The device is based on a photonic crystal waveguide: by combining the refractive index shift with slow-light enhanced absorption induced by free-carrier injection, we achieve an operation bandwidth that significantly exceeds the shift of the bandedge. We compare a 3 μm and an 80 μm long modulator and surprisingly, the shorter device outperforms the longer one. Despite its small size, the device achieves an optical bandwidth as broad as 7 nm for an extinction ratio of 10 dB, and modulation times ranging between 500 ps and 100 ps.

The desire for higher telecommunication bandwidth drives the quest for integrated photonic circuits. A key component of such circuits is the optical modulator[1], which has been realized in a variety of ways. Modulators typically use one of three approaches, i.e. either the absorption of light[2–4], a phase shift in conjunction with an interferometer[5–7], or the shifting of a resonance[8–14]. In all of these realizations there is a tradeoff between the different properties of modulators: the speed at which they operate, their energy consumption, their optical bandwidth, their footprints, and the ease with which they can be fabricated and integrated into existing circuits. For example, cavity based modulation is typically based on the shifting of extremely narrow resonances. Consequently, while such modulators allow for low energy consumption and fast operation, they are limited to very narrow optical bandwidths.

The tunability of the optical properties of two-dimensional photonic crystals (PhC) in conjunction with the maturity of silicon nanotechnology[1], makes their use as compact, ultrafast active elements extremely attractive. Recently, optical injection of free-carriers[15–17] in PhCs has enabled demonstrations of band-shifting[18], phase-changes[19] and frequency conversion[20]. In turn, these phenomena have been exploited for applications like directional couplers[21], the tunable delay of pulses[22] and modulators[11,19,23]. Proper dispersion engineering of photonic crystal waveguides, which enhances the light-matter interactions, has allowed for very compact[24] and very fast devices[25]. However, the PhC based modulators demonstrated so far, mostly depend on an interferometric design and still required relatively large footprints. What is missing is a design that allows for devices with a smaller footprint, yet with broad wavelength operation.

Here we use ultrafast pump-probe measurements to show that, using a PhC waveguide, it is possible to create an optical amplitude modulator that operates in transmission and that fulfils these requirements. We show that by exploiting the slow-light nature of the PhC waveguide[26,27], the footprint of the modulator can be reduced to an area of $\sim$10 μm^2 and that it is possible to significantly improve its performance. We offer a model that explains this surprising behaviour. Finally, we contrast our implementation with other realizations of optical modulators.

Results

Concept. Our modulator, which we show schematically in Fig. 1a, is based on bandshifting. That is, if the PhC waveguide is unpumped a mode is available for an input signal pulse and it is transmitted. Conversely, a control pump pulse can be used to optically inject free-carriers which shift the bandedge so that the mode is no longer available at the frequency of the input pulse. This pulse would then be reflected. As the carriers decay, the bandstructure shifts back towards its original state, allowing the signal to be transmitted again.

Bandshifting, however, is not the only effect in play. Signal light at wavelengths that are near the bandedge but too far away to be rejected by the bandshifting, experience strong changes in the group index (Fig. 1c). As we show

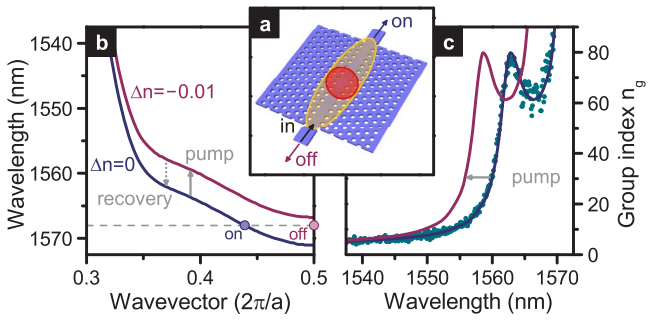

Figure 1 | Dispersion engineered photonic crystal modulator. (a) Schematic of the PhC modulator where the pumped area is represented by the yellow ellipse that covers the entire 80 μm waveguide or the red circle that covers a 3 μm section. The direction of the probe pulse is represented by the black arrow. (b) Calculated band structure of the unperturbed waveguide mode ($\Delta n = 0$) in blue and the perturbed waveguide mode ($\Delta n = -0.01$) in purple, with the 'on' and 'off' states labelled for a pulse centred at 1568 nm. (c) Group index of the waveguide mode as a function of freespace wavelength. The cyan dots represent the experimentally measured n_g of the unperturbed waveguide, whereas the thin lines are the calculated group indices corresponding to the dispersion shown in (b).

later, a large increase in the group index in combination with the presence of free-carriers can result in sufficient absorption of the signal light to effectively turn the transmission off. And, even more interestingly, this interplay between free-carrier absorption and group index change, results in different dynamics for differently sized structures.

To demonstrate this modulator we use an 80 μm long dispersion-engineered PhC waveguide, where the size and positions of the holes near the waveguide have been altered to create a flatband slow-light region[28–30]. In other words, the waveguide mode has a spectral region such that a relatively broadband pulse will experience a high group index yet relatively little group velocity dispersion. Such flatband regions are necessarily located away from the bandedge of the PhC waveguide mode, and as we show below, this spectral separation governs much of the modulation dynamics. Details on the design and fabrication can be found in ref. 31.

We present the calculated bandstructure of our unperturbed ($n_{Si} = 3.47, \Delta n = 0$) silicon PhC waveguide in Fig. 1b with the blue line[32]. To represent the perturbed waveguide we calculate the bandstructure for $n_{Si} = 3.46$ (i.e. $\Delta n = -0.01$). This bandstructure, indicated with the purple line in Fig. 1b, is blueshifted by ~4 nm with respect to the unperturbed bandstructure. This means that wavelengths in the range 1567 nm $< \lambda <$ 1571 nm would be transmitted through the unperturbed waveguide, but would be reflected from the waveguide when $\Delta n = -0.01$, as demonstrated for $\lambda = 1568$ nm in Fig. 1b by the dashed gray line.

In Fig. 1c we show the calculated group index, n_g, corresponding to the bandstructures shown in Fig. 1b, which we compare to our measured n_g, obtained using an interferometric measurement scheme[33]. This experimentally determined n_g of the unperturbed waveguide, which is depicted with cyan dots in Fig. 1c, is in good agreement with the calculated n_g.

Experiment. To experimentally investigate the dynamics of our modulator we use a pump-probe scheme, where we either pump the full length of the waveguide (80 μm), or pump a 3 μm section. The time delay between the pump and the telecom probe pulse is varied to map the transient response of the modulator. Figure 2 depicts the transmission of the waveguide as a function of pump-probe delay, measured at several wavelengths and normalized by the unpumped waveguide. Figure 2a shows the transmission when the full waveguide is pumped. The absorbed fluence (averaged over

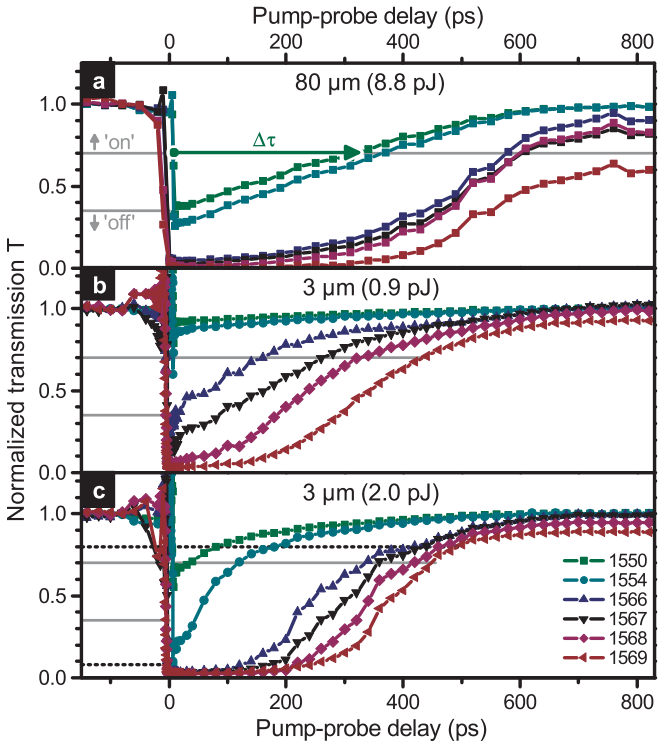

Figure 2 | Dynamics of the modulator. The transmission through the PhC waveguide as a function of the time delay for several different wavelengths, normalized by the transmitted intensity of the unpumped waveguide. (a) Transmission when the full length of the 80 μm waveguide is pumped. The absorbed energy is ~8.8 pJ. (b,c) Transmission when only a 3 μm section of the waveguide is pumped. The absorbed energy is ~0.9 pJ and ~2.0 pJ for (b) and (c) respectively. The solid gray lines indicate 35% and 70% transmission levels (3 dB ratio). The dotted black lines indicate 8% and 80% transmission levels (10 dB ratio). The green arrow in (a) illustrates the modulation time Δτ (for 1550 nm) as described in the Performance section of the text.

the 80 μm long waveguide and the 4 neighbouring rows to each side of the PhC) is ~37 fJ/μm^2, leading to an absorbed energy of ~8.8 pJ in the entire PhC waveguide.

The normalized transmission T at all the depicted wavelengths shows a sudden drop at zero time delay followed by a gradual recovery. The curious feature that T exceeds unity just before this drop is explained by the adiabatic frequency shifting of the probe pulse that occurs when the pump and the probe overlap in time[20]. The transmission of the shorter wavelengths drops to nonzero values and shows an immediate recovery whereas the transmission at the longest wavelengths drops to near-zero values and stays at this level for a couple hundred picoseconds before starting to recover.

This delay in recovery can be understood in terms of the pump induced shift of the bandstructure, and of the modegap in particular. Light that is initially near the cutoff, in this case 1568 and 1569 nm, ends up in the modegap due to the pumping and is therefore reflected. As the bandstructure begins to shift back due to carrier recombination, the shorter wavelengths, furthest from the original modegap, will be the first to be transmitted again. The longer wavelengths, closest to the original modegap, will be rejected the longest.

However, as explained above, bandshifting is not the whole story. The transmission at 1550 and 1554 nm is also reduced when the PhC is pumped, yet the bandshift is too small for these wavelengths to end up in the modegap. Three other mechanisms influence the transmission: free-carrier absorption, back-scattering and out-of-plane scattering, which scale with n_g, n_g^2 and n_g respectively[34,35]. Although, as we

will show later, the scattering losses turn out to be of less importance than the absorption losses.

These loss channels are the reason why the shorter wavelengths that are far away from the bandgap also exhibit a reduced transmission. To understand why the losses are higher for 1554 than for 1550 nm, we have to look at the group index. As can be seen in Fig. 1c, the group index of the pumped mode is almost twice as high at 1554 nm as it is at 1550 nm, resulting in higher absorption. For the longer wavelengths in Fig. 2a, where n_g is much higher, the absorption and scattering losses will be even more significant, strongly influencing the dynamics of the recovery.

It is clear from Fig. 2a, that while the 80 μm long waveguide can act like an optical modulator, its behaviour is far from ideal. In particular, the transmission recovers very slowly and the losses due to free-carrier absorption are high. This suggests that a shorter waveguide will perform superiorly as our modulator. This can be achieved by simply pumping a smaller section of the same waveguide. We expect this to highlight the effect of the bandshift rather than that of the absorption and scattering. In Fig. 2b we present the transmission when only a 3 μm section of the waveguide is pumped, with an average absorbed fluence of ~100 fJ/μm^2 leading to an absorbed energy of ~0.9 pJ. Although the absorbed fluence is almost 3 times higher than the case where the full waveguide is pumped, the absorbed energy is still 10 times lower than for the long modulator. In contrast to what we observed above (Fig. 2a), for the smaller pump spot the shortest wavelengths show very little losses, as a smaller total number of free-carriers are created, resulting in less absorption. The transmission at intermediate wavelengths (1566–1568 nm) drops to very low values but starts to recover immediately. Since these curves don't show the plateau at near-zero transmission, it is clear they are not being rejected by the mode-gap, but that their dynamics is governed by absorption losses. Transmission at 1569 nm drops to near-zero and remains there for ~100 ps before staring to recover. Clearly, pumping a smaller section results in lower absorption and, surprisingly, a quicker recovery. However, for the absorbed pump energy of 0.9 pJ only a very small wavelength range is suppressed to near-zero transmission. To suppress a larger range of wavelengths a higher pump energy is required.

In Fig. 2c we present the transmission when again a 3 μm section of the waveguide is pumped, but now with an average absorbed fluence of ~230 fJ/μm^2 leading to an absorbed energy of ~2.0 pJ. The transmission drops to near-zero for a much broader range of wavelengths than in the case where the full waveguide was pumped, but for a much lower absorbed energy. Further, the transmission recovers earlier and occurs in a much steeper fashion. This, surprisingly, suggests that a shorter modulator outperforms a longer one.

Performance. To compare the performance of the different realizations of the modulator in a more quantitative manner, we first define the modulation time $\Delta\tau$ as the time between the moment T drops below a lower threshold ('off' level) until the moment it exceeds an upper threshold ('on' level) again. The horizontal pair of solid gray lines in Fig. 2 indicates 'off–on' levels of 35%–70% (i.e. a ratio of 3 dB) and the dotted black lines indicates 8%–80% (10 dB ratio). Figure 3 shows the optical bandwidth $\Delta\lambda$, defined as the maximum continuous wavelength range that is accessible for a given modulation time. The blue, green and black sets of curves correspond to the data shown in Fig. 2a, 2b and 2c respectively. The solid and dotted curves correspond to the pairs of 'off' and 'on' levels of the same line style in Fig. 2.

A global increase of $\Delta\lambda$ as a function of $\Delta\tau$ time is observed, demonstrating the tradeoff between a short modulation time and a broad optical bandwidth. Comparing the different length modulators one can see that the long modulator (blue curve) is outperformed in $\Delta\lambda$ by the short modulator (solid black curve) for the whole wavelength range. Even at lower absorbed energy (green curve), the short

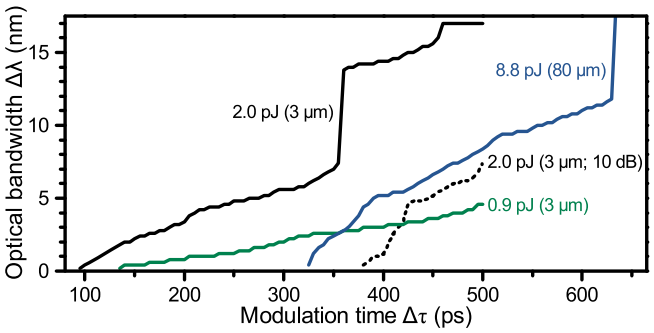

Figure 3 | The optical bandwidth $\Delta\lambda$ that can be modulated for given $\Delta\tau$. Extracted from the data presented in Fig. 2. All solid curves are for an extinction ratio of 3 dB, the dotted curves are for an extinction ratio of 10 dB. ($\Delta\tau$ is described in the Performance section of the text).

modulator allows for larger $\Delta\lambda$ up to $\Delta\tau$ = 350 ps, yet it demonstrates significantly narrower wavelength operation than the 2.0 pJ case (solid black). When increasing the extinction ratio from 3 dB (solid curves) to 10 dB (dotted curve) the optical bandwidth is much narrower, but $\Delta\lambda$ = 7 nm (5 nm) at $\Delta\tau$ = 500 ps (420 ps) can still be achieved for the 3 μm pump spot with an absorbed energy of 2.0 pJ (dotted black). However, an extinction ratio of 3 dB for the same pump spot (solid black) shows the best combination of optical bandwidth and modulation time with $\Delta\lambda$ =17 nm (14 nm) for $\Delta\tau$ = 480 ps (360 ps). This clearly demonstrates the benefit of pumping a smaller area, particulary considering the energy consumption is also much lower. Note that, at the cost of narrower optical bandwidth, higher insertion losses or a lower extinction ratio, smaller $\Delta\tau$ (down to 50 ps) could be achieved by a different choice of 'off–on' levels.

Model. To explain the dynamics of our modulator, we model our experiments as follows. The free-carrier concentration N follows directly from the absorbed fluence. Using the Drude model, the complex refractive index change of the silicon $\Delta\tilde{n}$ can be determined from N. For the concentrations that we are concerned with, $\Delta\tilde{n}$ scales linearly with N. The imaginary part of $\Delta\tilde{n}$ results in a free-carrier absorption coefficient α_{FC} for the transmitted light, and the real part, $\Delta n = \mathrm{Re}(\Delta\tilde{n})$ leads to a shift of the bandstructure. For the small Δn at which our device operates, the bandshift can be considered linear and constant for the wavelength range of interest. At wavelengths with low group velocity dispersion ($\lambda <$ 1540 nm) the phase shift will be proportional to the bandshift. By measuring the dynamics of the phase shift in an interferometric measurement scheme, we can determine a carrier decay time of ~350 ps. We can now determine α_{FC} and n_g as a function of delay time and wavelength. The absorption of the probe light is enhanced by the group index. This may be interpreted as the slowdown of light increasing the effective length of the waveguide by n_g/n_{Si}. The normalized transmission T can then be modelled as follows:

$$T(t) = \mathrm{e}^{-\alpha_{FC}(t)\frac{n_g(t)}{n_{Si}}L},$$

where L is the length of the pumped waveguide section (see Supplementary section Model and parameters). Losses due to back-scattering and out-of-plane scattering are neglected in this model, as we found that these are much smaller than the losses due to free-carrier absorption.

The modelled normalized transmission through a waveguide of length L = 80 μm and L = 3 μm is shown in Fig. 4a and Fig. 4b respectively. The group indices and α_{FC} are calculated for an absorbed fluence of 70 fJ/μm^2 (resulting in Δn = −0.01). A free-carrier decay time of 350 ps is assumed for both cases. The dashed

lines show the response of a spectral delta-peak and detail the response of a very narrowband source, the solid lines are transmission spectra that are convoluted with a 1 nm wide Gaussian to better represent our experiment.

The model shows good qualitative agreement with the measurements presented in Fig. 2. For the same absorbed fluence, we observe a faster recovery when a smaller section of the waveguide is pumped. The effect of the length of the waveguide on the recovery becomes even more obvious when looking at the single wavelength transmission (dashed curves) instead of the convoluted wavelength transmission (solid curves). The recovery of T when a 3 μm spot is pumped is very steep whereas the recovery when the full 80 μm long waveguide is pumped is very shallow, even though the same free-carrier recombination time was used.

The rejection of modes due to bandshifting is independent of the waveguide length, while the absorption is not. That is, if both the long and short waveguides are pumped at the same fluence, resulting in identical carrier concentrations, light in the 80 μm long waveguide will experience ~27 times more absorption than light in the 3 μm waveguide. Consequently, the recovery in the shorter waveguide, at a single wavelength, will occur almost instantaneously once the mode becomes available (Fig. 4b dashed curves). In contrast, the recovery in the longer waveguide will be far slower (Fig. 4a dashed curves), and will largely be dictated by the carrier recombination times. Note that this difference in response between the two waveguides is somewhat mitigated when we consider a more realistic pulse with a 1 nm bandwidth (solid curves in Fig. 4). However, as expected, even for this more realistic case, the transmission of the shorter waveguide recovers much more rapidly than that of the longer waveguide. In the experiment, the free-carrier recombination time would probably be shorter for the smaller pump spot due to diffusion of free-carriers out of the pumped area[14,36]. Note that our model does not take this effect into account, hence an even faster recovery may be expected for the small pump spot than our model predicts.

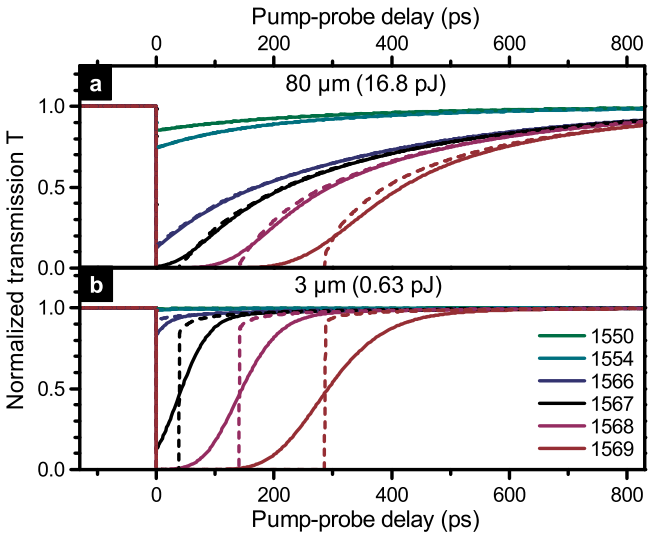

Figure 4 | Modelled dynamics of the modulator. Transmission as a function of time delay after pump pulse for several different wavelengths, normalized by the transmission of the unpumped waveguide. (a) Transmission when the full waveguide is pumped. (b) Transmission when only a 3 μm section is pumped. Both cases are modelled with the same absorbed pump fluence (70 fJ/μm^2) and hence also the same refractive index change ($\Delta n = -0.01$). The dashed curves show the transmission of a spectral delta peak, the solid curves represent the response of a 1 nm wide Gaussian.

Discussion

To conclude, we have demonstrated an ultrafast PhC based optical modulator that requires a footprint of only ~10 μm^2, yet can operate over a broad range of wavelengths. The device uses bandshifting to shift the modegap and to enhance propagation losses by slowing down the light. Shortening the length of the modulator not only reduces the energy consumption, but surprisingly also allows for shorter modulation times and larger optical bandwidth operation. Our device shows a high degree of flexibility. Depending on the requirements, one can pick between modulation times as short as 95 ps, an extinction ratio as high as 10 dB or an optical bandwidth as large as 17 nm. These operating limits could most likely be improved with a careful design of the dispersion relation. As mentioned above, the dominant loss mechanism in our modulator is slow-light enhanced free-carrier absorption, which scales with n_g. In the future, by combining a clever design of the bandstructure with an intentional increase in scattering losses, one can envision a modulator that relies on scattering losses which scale with n_g^2 (ref. 34), resulting in lower energy requirements (See Supplementary section Model and parameters).

Our silicon optical modulator compares favourably with those previously reported. It allows for much faster operation speed than is typical for devices using the thermo-optic effect (≳100 ns)[5] and in particular of those that rely on thermo-optic bandshifting (~100 μs)[37]. Electro-absorption modulators using the quantum-confined Stark effect achieve faster operation speeds and lower energy consumption[2,3], but require complex SiGe multilayers which are more difficult to fabricate and to integrate than silicon photonic crystal waveguides. Further, these electro-absorption modulators also suffer from higher insertion losses than photonic crystal waveguides. Both thermal and electro-absorption techniques require much larger footprints, as do Mach-Zehnder type modulators using carrier injection[6]. Modulators based on resonators such as Si microrings, can be achieved at a similar footprint[12] but their optical bandwidths are usually in the ~100 pm range. Combining the techniques from electro-absorption modulators with our PhC design might lead to the best of both worlds, i.e. compact design with broad wavelength operation combined with faster modulation and lower power consumption. Also note that the recovery time of our device could be significantly reduced by sweeping out the carriers with the p-i-n junction. Furthermore, such a junction could also be used to electrically pump this device, thereby achieving full integration. Modulation bandwidths as high as 40 Gbit/s have been achieved with electrically pumped Si photonic crystal waveguides[38]. In all, this is a compact and simple to fabricate[38] ultrafast optical modulator that joins other recent devices[13,14,19,21,22,25,39–43] in the toolbox for optical interconnects, as we progress towards optical information processing.

Methods

Sample fabrication. The fabrication of the PhC waveguide starts with a SOITEC silicon-on-insulator wafer consisting of a 220 nm Si layer on top of a 2 μm SiO_2 buffer layer. The required pattern is written in a layer of resist (ZEP520A) with an electron beam. The resist is developed using xylene with ultrasonic agitation[44] after which the pattern is transferred to the Si membrane using Reactive Ion Etching with CHF3 and SF6 gases[45]. To obtain a freestanding membrane, the silica underneath the PhC area is removed using Hydrofluoric acid (the remaining area being protected by photoresist). The result is an 80 μm long and 220 nm thick Si PhC waveguide surrounded by air[31]. Note that our device was not optimized to reduce insertion losses in the wavelength range where we operate. By clever design of the transition region from the access waveguide to the PhC waveguide, the coupling efficiency can be as high as 95% for a group index range as wide as 200 (ref. 46 and Supplementary section Transmission spectra).

Pump-probe experiment. To pump the structure, a 100 fs pulse from a 810 nm, 80 MHz Ti:Sapphire oscillator laser is focussed on the PhC, either in an elliptical spot of approximately 3 by 200 μm (FWHMI) to cover the full length of the waveguide (80 μm), or in a circular spot of 3 μm (FWHMI) as shown in Fig. 1a. Using the transfer matrix method, we calculate that about 1.4% of the incident pump light is absorbed in the Si membrane. The transmission of the PhC waveguide in the telecom wavelength range (near 1550 nm) is probed by a 140 fs broadband pulse. To avoid

nonlinear effects the intensity of the probe pulse is kept low. The time delay between the pump and the telecom probe pulse is varied by lengthening the path of the pump beam with a delay stage.

1. Reed, G. T., Mashanovich, G., Gardes, F. Y. & Thomson, D. J. Silicon optical modulators. *Nature Photon.* **4**, 518–526 (2010).
2. Feng, D. *et al.* High speed GeSi electro-absorption modulator at 1550 nm wavelength on SOI waveguide. *Opt. Express* **20**, 22224–22232 (2012).
3. Chaisakul, P. *et al.* 23 GHz Ge/SiGe multiple quantum well electro-absorption modulator. *Opt. Express* **20**, 3219–3224 (2012).
4. Asano, T., Tamura, M., Yoshizawa, S. & Noda, S. Pump-probe measurement of ultrafast all-optical modulation based on intersubband transition in n-doped quantum wells. *Applied Physics Letters* **77**, 19–21 (2000).
5. Vlasov, Y., O'Boyle, M., Hamann, H. & McNab, S. Active control of slow light on a chip with photonic crystal waveguides. *Nature* **438**, 65–69 (2005).
6. Gu, L., Jiang, W., Chen, X., Wang, L. & Chen, R. T. High speed silicon photonic crystal waveguide modulator for low voltage operation. *Appl. Phys. Lett.* **90**, 071105 (2007).
7. Liu, A. *et al.* A high-speed silicon optical modulator based on a metal-oxide-semiconductor capacitor. *Nature* **427**, 615–618 (2004).
8. Xu, Q., Schmidt, B., Pradhan, S. & Lipson, M. Micrometre-scale silicon electro-optic modulator. *Nature* **435**, 325–327 (2005).
9. Almeida, V. R., Barrios, C. A., Panepucci, R. R. & Lipson, M. All-optical control of light on a silicon chip. *Nature* **431**, 1081–1084 (2004).
10. Gardes, F. Y. *et al.* High-speed modulation of a compact silicon ring resonator based on a reverse-biased pn diode. *Opt. Express* **17**, 21986–21991 (2009).
11. Tanabe, T., Nishiguchi, K., Kuramochi, E. & Notomi, M. Low power and fast electro-optic silicon modulator with lateral p-i-n embedded photonic crystal nanocavity. *Opt. Express* **17**, 22505–22513 (2009).
12. Xu, Q., Fattal, D. & Beausoleil, R. G. Silicon microring resonators with 1.5-μm radius. *Opt. Express* **16**, 4309–4315 (2008).
13. Wülbern, J. H. *et al.* Electro-optic modulation in slotted resonant photonic crystal heterostructures. *Applied Physics Letters* **94**, 241107 (2009).
14. Nozaki, K. *et al.* Sub-femtojoule all-optical switching using a photonic-crystal nanocavity. *Nat Photon* **4**, 477–483 (2010).
15. Pankove, J. *Optical Processes in Semiconductors* (Dover Publications, New York, 1975).
16. Soref, R. & Bennett, B. Electrooptical effects in silicon. *IEEE J. Quantum Electron.* **23**, 123–129 (1987).
17. Euser, T. G. & Vos, W. L. Spatial homogeneity of optically switched semiconductor photonic crystals and of bulk semiconductors. *J. Appl. Phys.* **97**, 043102 (2005).
18. Leonard, S. W., van Driel, H. M., Schilling, J. & Wehrspohn, R. B. Ultrafast band-edge tuning of a two-dimensional silicon photonic crystal via free-carrier injection. *Phys. Rev. B* **66**, 161102 (2002).
19. Gu, L., Jiang, W., Chen, X., Wang, L. & Chen, R. T. High speed silicon photonic crystal waveguide modulator for low voltage operation. *Appl. Phys. Lett.* **90**, 071105 (2007).
20. Kampfrath, T. *et al.* Ultrafast adiabatic manipulation of slow light in a photonic crystal. *Phys. Rev. A* **81**, 043837 (2010).
21. Kampfrath, T. *et al.* Ultrafast rerouting of light via slow modes in a nanophotonic directional coupler. *Appl. Phys. Lett.* **94**, 241119 (2009).
22. Beggs, D. M. *et al.* Ultrafast Tunable Optical Delay Line Based on Indirect Photonic Transitions. *Phys. Rev. Lett.* **108**, 213901 (2012).
23. Jiang, Y., Jiang, W., Gu, L., Chen, X. & Chen, R. T. 80-micron interaction length silicon photonic crystal waveguide modulator. *Appl. Phys. Lett.* **87**, 221105 (2005).
24. Beggs, D. M., White, T. P., O'Faolain, L. & Krauss, T. F. Ultracompact and low-power optical switch based on silicon photonic crystals. *Opt. Lett.* **33**, 147–149 (2008).
25. Corcoran, B. *et al.* Optical signal processing on a silicon chip at 640 Gb/s using slow-light. *Opt. Express* **18**, 7770–7781 (2010).
26. Baba, T. Slow light in photonic crystals. *Nature Photon.* **2**, 465–473 (2008).
27. Krauss, T. F. Why do we need slow light? *Nature Photon.* **2**, 448–450 (2008).
28. Schulz, S. A. *et al.* Dispersion engineered slow light in photonic crystals: a comparison. *J. Opt.* **12**, 104004 (2010).
29. Kubo, S., Mori, D. & Baba, T. Low-group-velocity and low-dispersion slow light in photonic crystal waveguides. *Opt. Lett.* **32**, 2981–2983 (2007).
30. Monat, C. *et al.* Slow light enhancement of nonlinear effects in silicon engineered photonic crystal waveguides. *Opt. Express* **17**, 2944–2953 (2009).
31. Li, J., White, T. P., O'Faolain, L., Gomez-Iglesias, A. & Krauss, T. F. Systematic design of flat band slow light in photonic crystal waveguides. *Opt. Express* **16**, 6227–6232 (2008).
32. Johnson, S. & Joannopoulos, J. Block-iterative frequency-domain methods for Maxwell's equations in a planewave basis. *Opt. Express* **8**, 173–190 (2001).
33. Gomez-Iglesias, A., OBrien, D., OFaolain, L., Miller, A. & Krauss, T. F. Direct measurement of the group index of photonic crystal waveguides via Fourier transform spectral interferometry. *Appl. Phys. Lett.* **90**, 261107 (2007).
34. Hughes, S., Ramunno, L., Young, J. F. & Sipe, J. E. Extrinsic Optical Scattering Loss in Photonic Crystal Waveguides: Role of Fabrication Disorder and Photon Group Velocity. *Phys. Rev. Lett.* **94**, 033903 (2005).
35. O'Faolain, L. *et al.* Loss engineered slow light waveguides. *Opt. Express* **18**, 27627–27638 (2010).
36. Tanabe, T., Taniyama, H. & Notomi, M. Carrier diffusion and recombination in photonic crystal nanocavity optical switches. *Lightwave Technology, Journal of* **26**, 1396–1403 (2008).
37. Cui, Y., Liu, K., MacFarlane, D. L. & Lee, J.-B. Thermo-optically tunable silicon photonic crystal light modulator. *Opt. Lett.* **35**, 3613–3615 (2010).
38. Nguyen, H. C., Hashimoto, S., Shinkawa, M. & Baba, T. Compact and fast photonic crystal silicon optical modulators. *Opt. Express* **20**, 22465–22474 (2012).
39. Tanaka, Y. *et al.* Dynamic control of the Q factor in a photonic crystal nanocavity. *Nat Mater* **6**, 862–865 (2007).
40. Xia, F., Sekaric, L., O'Boyle, M. & Vlasov, Y. Coupled resonator optical waveguides based on silicon-on-insulator photonic wires. *Appl. Phys. Lett.* **89**, 041122 (2006).
41. Xu, Q., Shakya, J. & Lipson, M. Direct measurement of tunable optical delays on chip analogue to electromagnetically induced transparency. *Opt. Express* **14**, 6463–6468 (2006).
42. Beggs, D. M., Krauss, T. F., Kuipers, L. & Kampfrath, T. Ultrafast Tilting of the Dispersion of a Photonic Crystal and Adiabatic Spectral Compression of Light Pulses. *Phys. Rev. Lett.* **108**, 033902 (2012).
43. Kondo, K. *et al.* Ultrafast Slow-Light Tuning Beyond the Carrier Lifetime Using Photonic Crystal Waveguides. *Phys. Rev. Lett.* **110**, 053902 (2013).
44. Lee, K. L., Bucchignano, J., Gelorme, J. & Viswanathan, R. Ultrasonic and dip resist development processes for 50 nm device fabrication. *J. Vac. Sci. Technol. B* **15**, 2621–2626 (1997).
45. O'Faolain, L. *et al.* Low-loss propagation in photonic crystal waveguides. *Elec. Lett.* **42**, 1454–1455 (2006).
46. Hugonin, J. P., Lalanne, P., White, T. P. & Krauss, T. F. Coupling into slow-mode photonic crystal waveguides. *Opt. Lett.* **32**, 2638–2640 (2007).

Acknowledgments

This work is part of the research program of the Stichting voor Fundamenteel Onderzoek der Materie (FOM), which is financially supported by the Nederlandse Organisatie voor Wetenschappelijk Onderzoek (NWO). The work is also supported by the research programs NanonextNL and MEMPHIS, funded by the Dutch ministry of economic affairs. We also acknowledge financial support by the EPSRC through the "UK Silicon Photonics" grant.

Author contributions

The initial concept was conceived by N.R. and D.M.B. and was expanded by T.F.K., A.O. and L.K. The device was fabricated by I.H.R. and T.F.K. The experiments and analysis of the data were performed by A.O. with support from N.R., D.M.B. and L.K. All authors contributed to the manuscript.

Additional information

Supplementary information accompanies this paper at http://www.nature.com/scientificreports

Competing financial interests: The authors declare no competing financial interests.

How to cite this article: Opheij, A. *et al.* Ultracompact (3 μm) silicon slow-light optical modulator. *Sci. Rep.* **3**, 3546; DOI:10.1038/srep03546 (2013).